Int. J. Electrochem. Sci., 14 **(2019)** 4974 – 4985, doi: 10.20964/2019.06.43

International Journal of
ELECTROCHEMICAL
SCIENCE
www.electrochemsci.org

A Self-Recoverable $LiTi_2(PO_4)_3/O_2$ Hybrid Cathode for Lithium-Oxygen Batteries with High Power Performance

Zhendong Ding[1], *Shijia Mu*[1], *Ding Zhu*[2,*], *Yungui Chen*[1,*]

[1] College of Materials Science and Engineering, Sichuan University, Chengdu 610065, PR China
[2] Institute of New Energy and Low-Carbon Technology, Sichuan University, Chengdu 610065, PR China
[*]E-mail: 504420809@qq.com; ygchen60@aliyun.com

Received: 5 January 2019 / *Accepted:* 12 March 2019 / *Published:* 10 May 2019

Despite the potential of delivering desirably high energy, the wide application of lithium-oxygen batteries (LOBs) is severely restricted by its poor power performance. In this study, a $LiTi_2(PO_4)_3/O_2$ hybrid cathode was constructed, in which the carbon-coated $LiTi_2(PO_4)_3$ was prepared by a sol-gel method. Comparing to conventional LOB cathode, the $LiTi_2(PO_4)_3/O_2$ hybrid cathode (LOHC) exhibited considerable power density as high as 5.5 $mW \cdot cm^{-2}$ (more than 4 times of LOB cathode power density) at high currents up to 4 $mA \cdot cm^{-2}$ while retaining high-energy delivery at low currents. It also showed the ability of self-recovery to charged-state in the environment of oxygen (the capacity recovery percentage stayed around 80% in each resting process), which improved the high-power output durability. This work may provide a new approach to promote the development of lithium-oxygen batteries.

Keywords: Li-O_2 battery; $LiTi_2(PO_4)_3$; high power output; self-recovery

1. INTRODUCTION

To meet the rapidly growing demands of energy storage, lithium ion batteries (LIBs) are playing an important role in the consumer market among today's power sources [1-3]. However, it fails to extend its further utilizing in high-energy demanding areas because of its insufficient energy density, which limits the development of cellphones, electric vehicles and other products [4-5]. Researchers developed some novel battery systems to achieve a higher energy density, and among which lithium-oxygen batteries (LOBs) attracts considerable attention as a promising solution to the problem [6-7]. Theoretically, LOBs deliver a significantly high gravimetric energy density of ~3500 $Wh \cdot kg^{-1}$ [8-11] which is nearly 10 times higher than its counterpart of LIBs. However, the further application of LOBs

stands confronted by a series of critical issues particularly led by the unsatisfying performance of the O_2 cathode, such as the poor power performance [12-17], especially in the automotive field.

There are several reasons attributing to the low power output of LOBs. The first is the very low ionic/electronic conductivity of the Li_2O_2 produced during the oxygen reduction reaction (ORR, $O_2 + 2Li^+ + 2e^- \rightarrow Li_2O_2$) occurred at the cathode [14], [18-19], and this discharge product Li_2O_2 causes the charge transport through the bulk Li_2O_2 to the cathode-electrolyte reaction interface to be extremely low. Secondly, the charge transfer reaction at the Li_2O_2/electrolyte interface may also be retarded, for there is yet no proof showing an apparent ORR catalysis of Li_2O_2. Moreover, the ORR rate is restricted by the slow diffusion of O_2 in organic electrolyte [20-22], which increases the cathode polarization. Researcher have put a lot of efforts in promoting the charge transfer[18-19], the diffusion of oxygen[20-22] and the ORR catalysis[16-17, 23-24]. Lu et al.25 showed that the power performance of the oxygen cathode was improved by the faster lithium ion transport in defective Li_2O_2. Zhang et al.[22] designed a carbon-nanotubes/ionic liquid gel to build faster transporting passages for oxygen. And there are many researchers focusing on introducing novel ORR catalysts to enhance the power output [16-17, 23-24].

We hereby present a new idea in improving the power performance of LOBs. A $LiTi_2(PO_4)_3/O_2$ hybrid cathode (LOHC) has been established by introducing carbon-coated $LiTi_2(PO_4)_3$, a Na-super-ionic-conductor (NASICON)-type inorganic material, into the O_2 cathode of LOBs. $LiTi_2(PO_4)_3$ is employed because of the fast ion transport and long lithiation/delithiation cycle life brought by the highly stable three-dimensional NASICON framework[26] and its appropriate lithiation potential (2.54 V vs. Li/Li^+, slightly lower than the ORR potential)[27] for the hybrid cathode. There are two reduction reactions occurring in the cathode during the discharge process, including the $LiTi_2(PO_4)_3$ lithiation ($LiTi_2(PO_4)_3 + 2Li^+ + 2e^- \rightarrow Li_3Ti_2(PO_4)_3$) and the ORR ($O_2 + 2Li^+ + 2e^- \rightarrow Li_2O_2$). With the potential slightly lower than that of the ORR, the fast Li^+ insertion in $LiTi_2(PO_4)_3$ takes priority over the ORR and enables the LOHC to exhibit a lower overpotential than that of the ORR at high current densities, and thus enhance the battery power output. While discharging at low currents, the ORR mainly occurs at the cathode and assures that the LOHC deliver nearly comparable energy to that of common LOBs.

2. EXPERIMENTAL

2.1. Material synthesis

The carbon-coated $LiTi_2(PO_4)_3$ powder was prepared by a sol-gel method, in which the synthesis of $LiTi_2(PO_4)_3$ and the carbon coating process were carried out at the same time. Firstly, polyvinyl alcohol (PVA)-1788 was dissolved in water to prepare a 2 wt % PVA aqueous solution. The solution was slowly stirred for about 4 hours until the solution became fully clear. Li_2CO_3, $NH_4H_2PO_4$ and $Ti(OBu)_4$ of stoichiometric ratio were added into the solution, and the mixture was stirred slowly at a constant temperature of 80°C until the water was completely evaporated and a white solid precursor formed. Afterwards the product was transferred in a porcelain boat, put in a tube furnace and maintained at 800°C for 8h at a heating rate of 5°C min^{-1} under Ar flow. After the furnace cooled down, the precursor turned into black powder and was fully ground for the next experiments.

2.2. Characterization

X-ray diffraction (XRD) of the as-prepared powder was conducted with $Cu_{K\alpha}$ radiation in a Dandong DX-2600 X-ray diffractometer. Thermogravimetric analysis (TGA) of the carbon-coated $LiTi_2(PO_4)_3$ was performed with a Mettler 1100LF thermal analyzer. Scanning electron microscopy (SEM) images were obtained with an FEI Inspect F50. Transmission electron microscopy (TEM) was carried with a FEI Titan G2 60-300. X-ray photoelectron spectroscopy (XPS) was performed with a Thermo Scientific Escalab 250Xi.

2.3. Electrochemical tests

In a typical process of preparing a $LiTi_2(PO_4)_3/O_2$ hybrid cathode, a nickel foam disc with a diameter of 14 mm and a thickness of around 150 μm was used as the current collector. The LOHC was fabricated by pasting a mixture of Super P carbon (90 wt %) as the ORR sites provider and polyvinylidene fluoride (PVDF, 10 wt %) as the binder onto one side of the current collector (the oxygen side), and pasting a mixture of carbon-coated $LiTi_2(PO_4)_3$ as the active material, acetylene black as the conductive additive and PVDF as the binder with a gravimetric ratio of 80:15:5 onto the other side of the current collector (the separator side). In the case of a $LiTi_2(PO_4)_3$ cathode or a O_2 cathode, there is only a mixture of carbon-coated $LiTi_2(PO_4)_3$, acetylene black and PVDF or a mixture of Super P carbon and PVDF pasted respectively. After the mixture was pasted, the cathode was dried in vacuum at 120°C for 12h.

Swagelok-type Li-O_2 batteries were assembled in a glove box filled with pure argon gas. A lithium foil was used as the anode and a Celgard 2500 membrane as the separator in each battery. The electrolyte was 0.8 M lithium bis(trifluoromethanesulfonyl)imide (LiTFSI) dissolved in tetraethylene glycol dimethyl ether (TEGDME). The as-assembled Li-O_2 batteries were tested under pure oxygen (1 atm) with Land Battery Testing System (Wuhan Land Electronic Co. Ltd.).

3. RESULTS AND DISCUSSION

3.1. Characterizations of the as-prepared carbon-coated $LiTi_2(PO_4)_3$ powder

Fig. 1a is the XRD pattern of prepared $LiTi_2(PO_4)_3$ powder, in which the main peaks are well indexed in the hexagonal crystal system (space group *R*3c, JCPDS card #35-0754). And the morphology of the $LiTi_2(PO_4)_3$ particles is displayed in Fig. 1b and Fig. 1c, which reveal the individual particles with submicron size. The TGA curve in Fig. 1d indicates that the carbon content in the sample accounts for about 11%. The TEM images of Fig. 1e and Fig. 1f demonstrate a thin carbon layer of 6-9 nm thick on the surface of the $LiTi_2(PO_4)_3$ particles(the carbon coat displays as the light grey semitransparent part in Fig. 1e and the non-uniform layer in Fig. 1f), which can effectively make up for the cathodic electronic conductivity. Compared to the particle with lattice fringes, the carbon layer is apparently amorphous and non-uniform along the whole surface. In the HRTEM, the lattice spacing of 0.44 and 0.19 nm can be

respectively matched with {1 0 4} and {1 3 4} crystal planes, indicating that the $LiTi_2(PO_4)_3$ phase is pure.

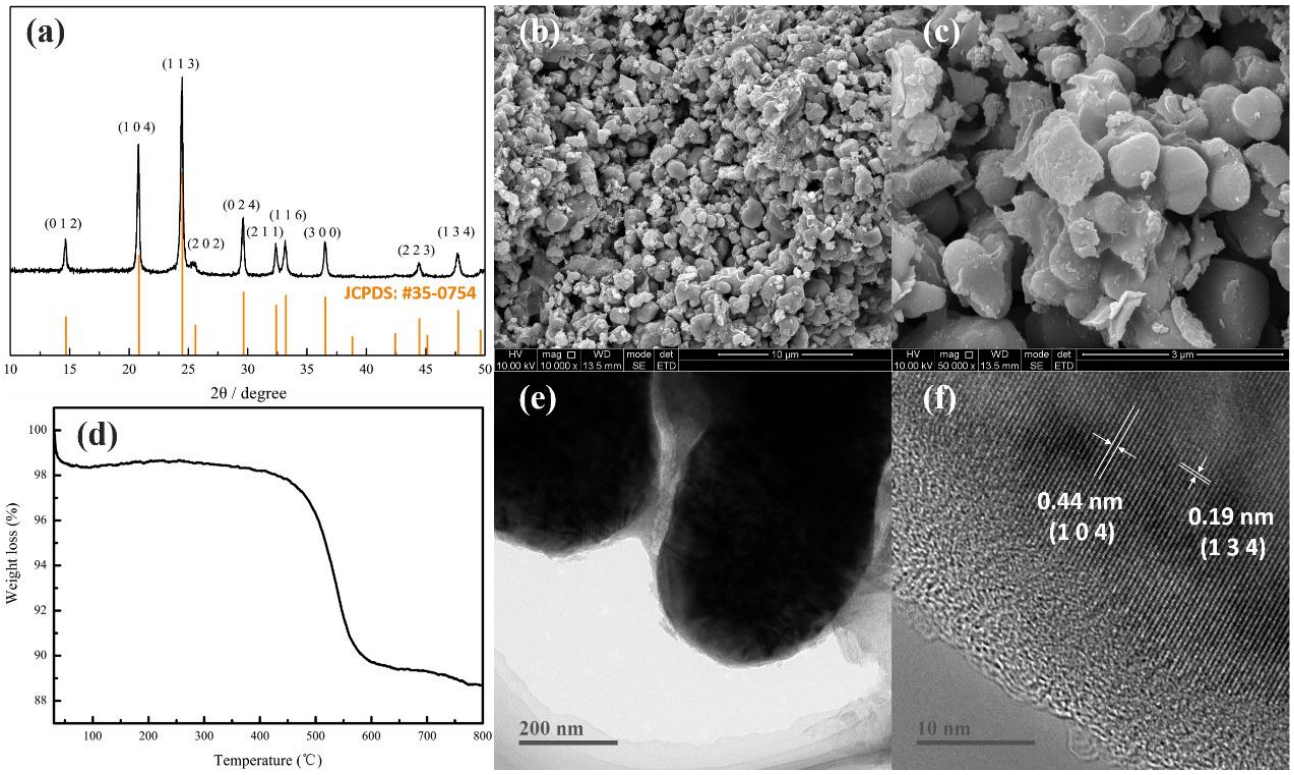

Figure 1. Characterizations of the as-prepared carbon-coated $LiTi_2(PO_4)_3$ powder: (a) XRD pattern; (b, c) SEM images; (d) TGA curve; (e) TEM image and (f) HRTEM image

3.2. Working principle of the hybrid cathode

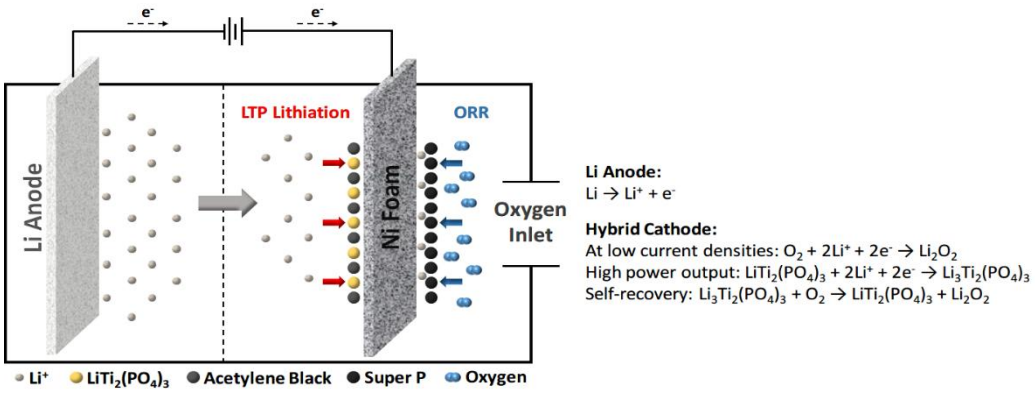

Figure 2. The design and principle of Li-O_2 battery with $LiTi_2(PO_4)_3/O_2$ hybrid cathode

As shown in Fig.2, the ORR side of the $LiTi_2(PO_4)_3/O_2$ hybrid cathode (LOHC) is covered with Super P carbon, which allows ORR to occur at a large number of reaction sites to deliver most of the energy. The other side of the LOHC is covered with carbon-coated $LiTi_2(PO_4)_3$, which plays an important role in discharging at a relatively higher power with the $LiTi_2(PO_4)_3/Li_3Ti_2(PO_4)_3$ redox reactions. To reduce the distance of oxygen diffusion, the Super P carbon is closer to the oxygen inlet, while the $LiTi_2(PO_4)_3$ is facing the Li anode to promote the $LiTi_2(PO_4)_3$ lithiation and avoid the passivation brought by the discharge product Li_2O_2 in the oxygen side. While the LOHC is discharging at a low current density, it is the ORR instead of the $LiTi_2(PO_4)_3$ lithiation that primarily occurs, since the working potential of the ORR ($O_2 + 2Li^+ + 2e^- \rightarrow Li_2O_2$, E^0=2.96 V, the discharge potential vs. Li/Li^+ is generally around 2.7V[11]) stands higher than that of the $LiTi_2(PO_4)_3$ lithiation ($LiTi_2(PO_4)_3 + 2Li^+ + 2e^- \rightarrow Li_3Ti_2(PO_4)_3$, the redox potential vs. Li/Li^+ is 2.54 V[27]). In the cases of high current densities, it is the $LiTi_2(PO_4)_3$ lithiation mostly occurring in the cathode, because the polarization of ORR is much more severe than that of the $LiTi_2(PO_4)_3$ lithiation, so that the operating potential of the latter stays higher than that of the ORR. Furthermore, the redox potential of the reaction between $Li_3Ti_2(PO_4)_3$ and oxygen ($Li_3Ti_2(PO_4)_3 + O_2 \rightarrow LiTi_2(PO_4)_3 + Li_2O_2$) is calculated to be 0.42 V from the above-mentioned two reactions, which theoretically indicates that the self-recovery from $Li_3Ti_2(PO_4)_3$ to $LiTi_2(PO_4)_3$ occurs spontaneously in oxygen atmosphere. Consequently, the $LiTi_2(PO_4)_3$ side and the Super P carbon side are capable to provide with high power output and high energy output separately for external loads.

3.3. Electrochemical performance

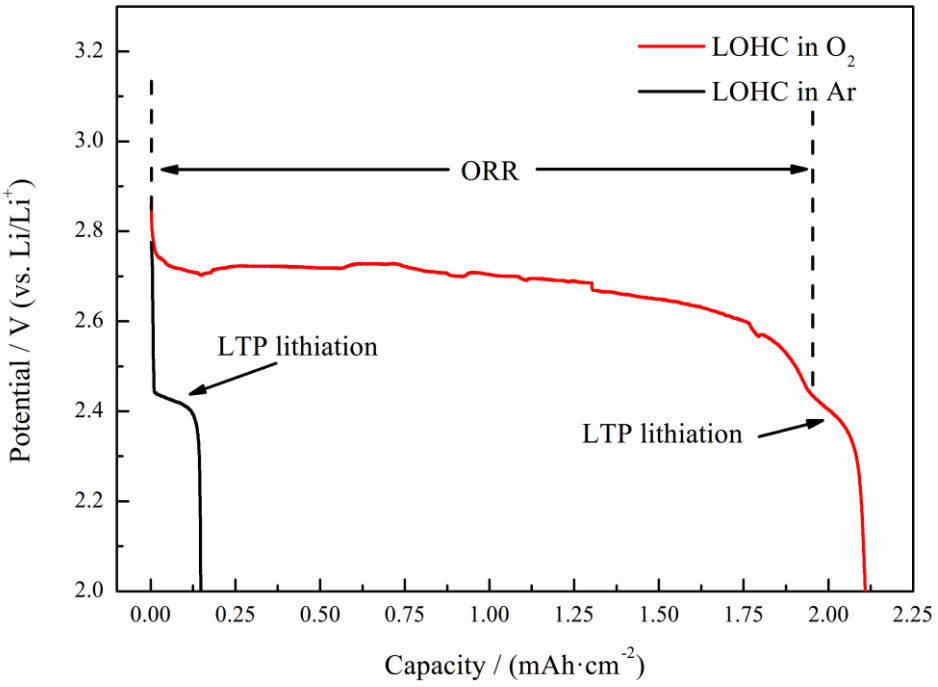

Figure 3. Discharge curves of the LOBs with LOHC in O_2 (the red curve) and in Ar (the black curve) at 0.01 $mA \cdot cm^{-2}$

Discharge curves of the Li-O_2 batteries with $LiTi_2(PO_4)_3/O_2$ hybrid cathode are illustrated in Fig. 3. In this test, one sample was discharging in oxygen to exhibit the ORR potential and capacity, and the other was discharging in argon to compare with the sample in oxygen, so that the capacity delivered by ORR was excluded. The current density in both tests was set at 0.01 $mA \cdot cm^{-2}$, and the specific capacity was calculated based upon the one-sided area of the cathode (regarded as a disc with a diameter of 14 mm). It is noted that there were two plateaus in the discharge process of the LOHC in O_2. The first was around 2.6 V vs. Li/Li^+. It was in accordance with the potential of ORR as mentioned above in 3.2 [11]. This voltage plateau is also observed in the work of Peng et al.[17] and Wu et al.[28], in which they adopted the same active cathode material (Super P carbon), and the ORR discharge potentials were both about 2.6 V vs. Li/Li^+ in their work. The ORR contributed far more energy than the second reaction (the Li^+ insertion into $LiTi_2(PO_4)_3$ at a potential of 2.5~2.4 V). The second plateau is identical to the potential of $LiTi_2(PO_4)_3$ lithiation according to the Delmas et al.'s research[27]. From the figure we can see that the $LiTi_2(PO_4)_3$ lithiation plateau was the only discharge plateau observed during the discharge of the LOHC in argon. As the figure shows, the ORR delivered a capacity of nearly 1.9 $mAh \cdot cm^{-2}$, while the $LiTi_2(PO_4)_3$ lithiation only delivered a capacity of about 0.15 $mAh \cdot cm^{-2}$. Furthermore, it can be observed that while discharging at a low current density like 0.01 $mA \cdot cm^{-2}$, the ORR takes priority over the $LiTi_2(PO_4)_3$ lithiation in LOHC, so that the LOB with LOHC retained the advantage of high energy density in conventional LOBs.

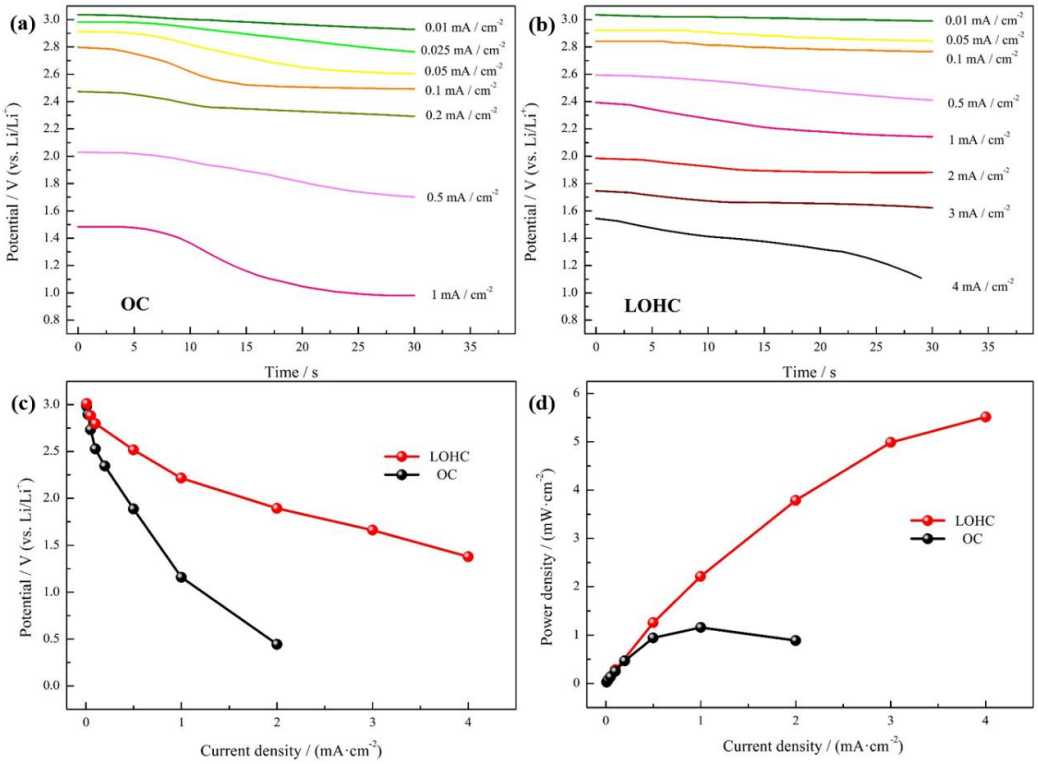

Figure 4. 30s-discharge tests of the LOBs with LOHC and OC: (a) 30s-discharge curves of LOBs with OC and (b) LOHC at different current densities; (c) median potential curves and (d) power density curves

To confirm that the power output in LOHC is higher than that in conventional oxygen cathode (OC) at higher rates, 30s-discharge curves were attained through intermittent discharging tests to visibly demonstrate the overpotential at different current densities of each cathode (Fig. 4a and Fig. 4b). Despite the fact that the potential of ORR (about 2.7 V vs. Li/Li^+) is higher than that of $LiTi_2(PO_4)_3$ lithiation (about 2.45 V vs. Li/Li^+), it is apparent that the practical potential of the LOHC is higher than its counterpart of the OC at current densities quite higher than 0.1 $mA \cdot cm^{-2}$. With the current density set higher, the difference between their potentials became greater. For example, while discharging at current densities of 0.1 $mA \cdot cm^{-2}$ and 1 $mA \cdot cm^{-2}$, the LOHC discharging curves showed two plateaus of 2.8 V and 2.2 V respectively, and in the case of OC they were 2.6 V and 1.2 V respectively. At a current density of as high as 4 $mA \cdot cm^{-2}$, the LOHC still worked with a potential vs Li/Li^+ of about 1.3 V while the OC was unable to discharge, proving that the LOHC shows a much better power performance than the OC. The power output of LOHC is also higher than other researchers' work[15, 25, 29] according to the power calculated based on the current collector area. For example, in Lu et al.'s work [25], Au-catalyzed Vulcan carbon was introduced to elevate the discharge voltage of Li-O_2 batteries while discharging at high rates. When discharging at 0.1 $mA \cdot cm^{-2}$, they lifted the voltage to around 2.6 V (in comparison it was 2.8 V in our work of LOHC); when it comes to 0.3 $mA \cdot cm^{-2}$, their voltage was 2.5 V (it was about 2.7 V in our work). In conclusion, introducing LOHC into Li-O_2 batteries indeed lifts the discharging voltage and improves the power performance.

Fig. 4c presents the median potential - current density curves of this discharging test and Fig. 4d is the power density - current density curve. It can be clearly seen from these figures that the differences in potential and power between LOHC and OC increase rapidly with the current increasing, therefore the advantage in power output of LOHC at high rates stands significant over the OC. For instance, while discharging at current densities of 1 $mA \cdot cm^{-2}$ and 2 $mA \cdot cm^{-2}$, the LOHC showed a power density of 2.2 $mW \cdot cm^{-2}$ and 3.8 $mW \cdot cm^{-2}$ respectively, while in the case of OC they were 1.1 $mW \cdot cm^{-2}$ and 0.9 $mW \cdot cm^{-2}$ respectively. The power density of LOHC is also considerably high comparing to other researchers' results[25][30]. For instance, in the research work of Zhao et al.[30], 3D porous N-doped graphene aerogels were employed to enhance the rate performance of Li-O_2 batteries. While discharging at a large current density of 1 $A \cdot g^{-1}$, their Li-O_2 aerogels system delivered a high power density of 1451 W/kg, and our LOHC system delivered a power density of about 2400 W/kg (converted by the mass load). And the mass load of our LOHC was nearly twice as much as theirs (0.61 $mg \cdot cm^{-2}$), indicating that the LOHC may exhibit even a higher power density if the mass load is reduced to 0.61 $mg \cdot cm^{-2}$. Additionally, we can also see that the peak power density of the LOHC was presented at a current density of around 4 $mA \cdot cm^{-2}$, while in the case of the OC it was only around 1 $mA \cdot cm^{-2}$. Consequently, it is ascertained that the introduction of $LiTi_2(PO_4)_3$ enables the cathode to operate with higher power than LOB cathode.

3.4. Self-recovery

Compared to the ORR, the $LiTi_2(PO_4)_3$ lithiation is much lower in terms of capacity, yet the discharge product $Li_3Ti_2(PO_4)_3$ can be oxidized easily while the ORR product Li_2O_2 can hardly be

oxidized to recover to charged state. According to the researchers' work in energetics theories, Abraham et al.[11,31] found that the equilibrium potential of Li_2O_2-generated ORR is E^0=2.96 V ($O_2 + 2Li^+ + 2e^- \rightarrow Li_2O_2$) , and Delmas et al.[27] found that the redox potential vs. Li/Li^+ of $LiTi_2(PO_4)_3$ ($LiTi_2(PO_4)_3 + 2Li^+ + 2e^- \rightarrow Li_3Ti_2(PO_4)_3$) is 2.54 V.

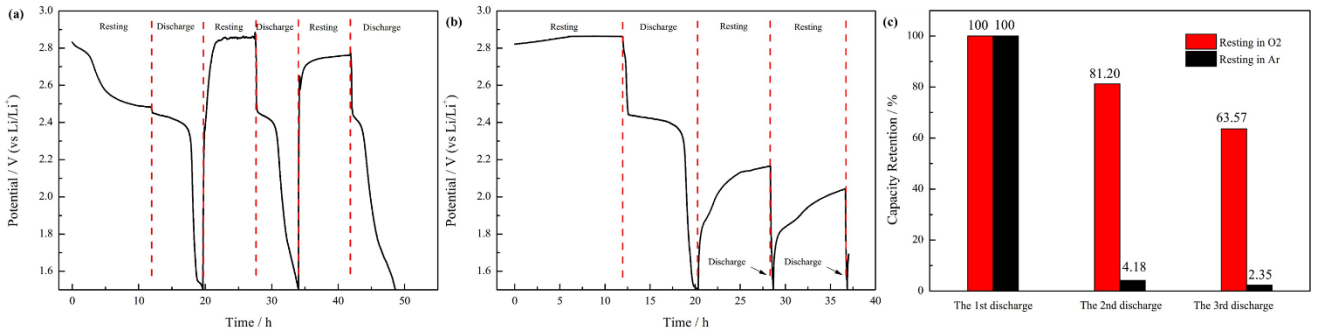

Figure 5. Discharge/resting cycle curves of the LOBs with LOHC: (a) discharge/resting cycle curve of the LOB with LOHC in oxygen and (b) argon; (c) capacity retention in each discharge/resting cycle of the LOBs with LOHC in oxygen and argon

Therefore, the redox potential of the reaction between $Li_3Ti_2(PO_4)_3$ and oxygen ($Li_3Ti_2(PO_4)_3 + O_2 \rightarrow LiTi_2(PO_4)_3 + Li_2O_2$) is calculated to be 0.42 V from the above-mentioned two reactions based on the Gibbs free energy $\triangle G = -nFE$, which indicates that the self-recovery from $Li_3Ti_2(PO_4)_3$ to $LiTi_2(PO_4)_3$ occurs spontaneously in oxygen atmosphere in energetics[27,31]. Hence through the regeneration of $LiTi_2(PO_4)_3$, the LOHC is capable of providing high power output for a long period of time instead of a single round of high-powered discharging. The resting-discharging test was carried out to observe the self-recovery of capacity and there was no charging but only discharging and resting in the test procedure. As Fig. 5a demonstrates, the resting-discharging test of LOHC shows that the capacity of LOHC has recovered to some extent via resting in oxygen atmosphere, and each discharge process was similar in the aspect of potential and the shape of curve. As the LOHC rested in oxygen, the potential nearly recovered to the open circuit potential observed before discharging, and the stable potentials in the resting parts decreased as the rounds proceeding. In comparison, the LOHC resting in argon atmosphere displayed little recovered capacity with nearly no discharge voltage plateau but only a sharp drop in potential as Fig. 5b illustrates. As for the resting process, the potentials in argon case also showed a similar decreasing trend with the oxygen case, but the stable potentials were obviously lower and the recovery proceeded much slower than in oxygen.

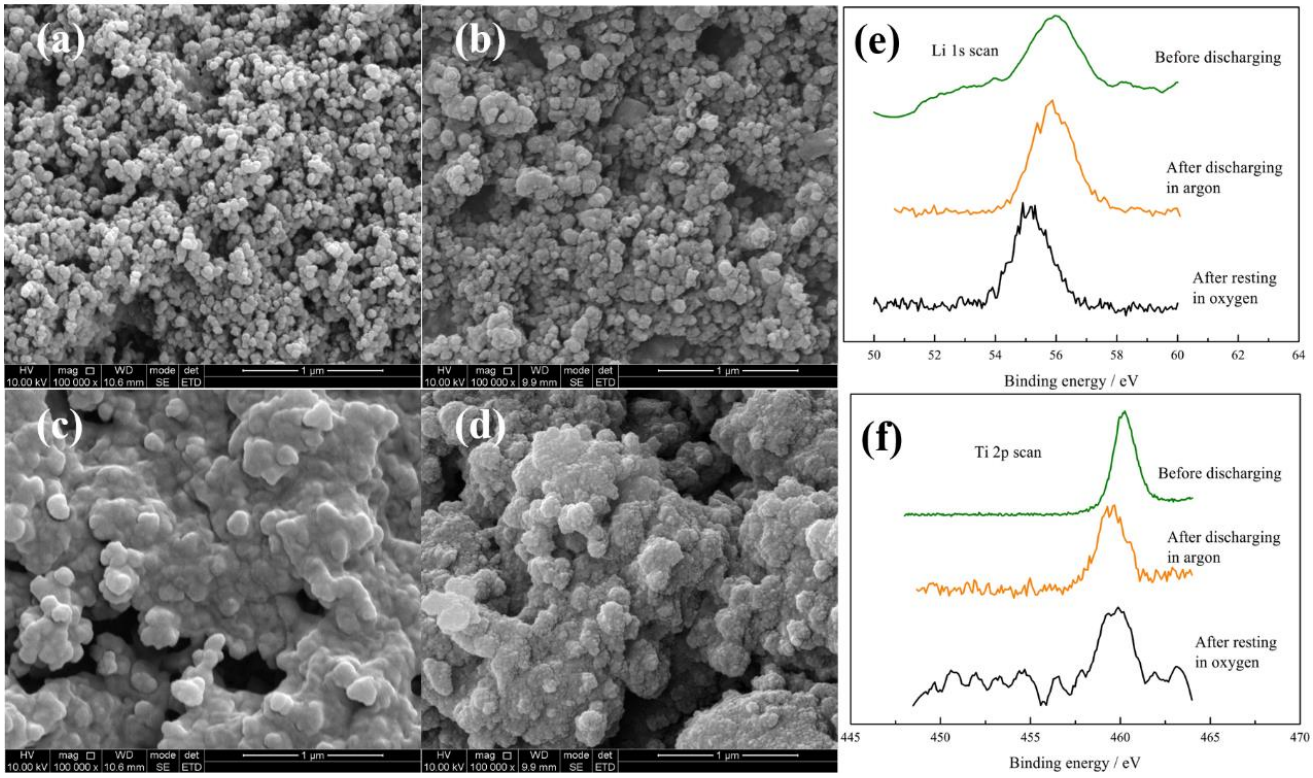

Figure 6. Self-recovery characterizations: (a) SEM images of the ORR side and (b) the $LiTi_2(PO_4)_3$ side of the LOHC before tests; (c) SEM images of the ORR side and (d) the $LiTi_2(PO_4)_3$ side after discharged in argon and then resting in oxygen; (e) the XPS spectra of the LOHC ($LiTi_2(PO_4)_3$ side) by Li 1s scan and (f) Ti 2p scan

The capacity retention in each round was calculated and revealed in Fig. 5c. After a resting process in oxygen of 8 hours, the capacity of the second round discharge was 81.20% of the first discharge, while after resting in argon for 8 hours the capacity of the second round discharge was only 4.18% of the first discharge in comparison. The third discharge also showed a similar pattern, in which the capacity of LOHC in oxygen was 63.57% of the first discharge, and the OC was only 2.35%. It was calculated that the capacity recovery stayed around 80% in each round of resting and discharging. Apparently, the existence of oxygen is crucial to the delithiation of $Li_3Ti_2(PO_4)_3$, thereby realizes the self-recovery of $LiTi_2(PO_4)_3$ and secures the sustained high-power output.

As mentioned above in the first paragraph of 3.4, there are two possible mechanisms of the spontaneous $Li_3Ti_2(PO_4)_3$ delithiation while resting in oxygen based on the researchers' work in energetics [27,31]. The first is that the discharged state cathode material $Li_3Ti_2(PO_4)_3$ on the separator side of LOHC directly contacts with the oxygen diffusing through the cathode from the other side and reacts with it ($Li_3Ti_2(PO_4)_3 + O_2 \rightarrow LiTi_2(PO_4)_3 + Li_2O_2$, E^0=0.42 V). If it happens, the delithiation product Li_2O_2 will appeared in situ on the $LiTi_2(PO_4)_3$ side. This mechanism is referred to as "chemical oxidation". The other mechanism is that the $Li_3Ti_2(PO_4)_3$ on the separator side and the oxygen on the ORR side jointly constitute a micro-battery with different equilibrium potentials of these two electrodes[11,27]. In the micro-battery model, the $Li_3Ti_2(PO_4)_3$ and oxygen works respectively as the anode and the cathode. Through the "short-circuit" of the micro-battery (the anode and cathode are both

on the current collector so that the short-circuit occurs), electrons transfer from the $Li_3Ti_2(PO_4)_3$ to oxygen, and therefore the oxidation of the $Li_3Ti_2(PO_4)_3$ and reduction of oxygen occurs. This mechanism is referred to as "electrochemical oxidation". Compared to the "chemical oxidation", this mechanism operates much rapidly. Because the "chemical oxidation" must proceed with the slow oxygen dissolution in the electrolyte and long-ranged oxygen diffusion, but the "electrochemical oxidation" runs through only the short-ranged Li^+ diffusion through the cathode. Besides, in "electrochemical oxidation" the oxidation product Li_2O_2 is deposited on the ORR side where the oxygen accept the electrons and react with the Li^+ diffusing from the $Li_3Ti_2(PO_4)_3$. With produced Li_2O_2 covering the ORR side rather than the $LiTi_2(PO_4)_3$ side, there is much less passivation brought to $LiTi_2(PO_4)_3$ in "electrochemical oxidation" and it is beneficial to the recovery life of $LiTi_2(PO_4)_3$.

To determine the actually happened mechanism, SEM imaging and XPS analysis were conducted. Fig. 6a shows the ORR side (covered with Super P carbon) of the LOHC and Fig. 6b shows the $LiTi_2(PO_4)_3$ side before electrochemical tests. The morphology of these two side of Super P and $LiTi_2(PO_4)_3$ are also separately observed in the work of Xiao et al.[32] and Luo et al.[33], in which they also noticed the same electrode surface morphology and identified the Super P and $LiTi_2(PO_4)_3$ respectively. The ORR side and $LiTi_2(PO_4)_3$ side after discharged in argon and then resting in oxygen are illustrated in Fig. 6c and Fig. 6d respectively. The Super P side morphology after discharging and resting in oxygen was also observed in Read's research about characterization of discharged PTFE/Super P air cathode of Li-O_2 batteries[34], and the product was confirmed to be Li_2O_2 by his characterization. The recovery mechanism can be observed through the surface morphology in SEM images, because the side where Li_2O_2 appears is different in these two mechanisms. As the figures demonstrate, it was less rougher on the $LiTi_2(PO_4)_3$ surface and more intact on the ORR side after the self-recovery. This distinctive change in morphology indicated that there was Li_2O_2 produced after resting in the oxygen, which was in agreement with the "electrochemical oxidation" mechanism. Likewise, there was also obvious aggregation on the $LiTi_2(PO_4)_3$ side. This was also caused by the Li_2O_2 produced by the $Li_3Ti_2(PO_4)_3$ – oxygen reaction. Thus the existence of the "chemical oxidation" was also noticed here. In comparison, the morphology change on the ORR side appeared more noticeable, indicating that the "electrochemical oxidation" was the dominating reaction during the self-recovery process. This phenomenon was beneficial to the LOHC self-recovery life since the "chemical oxidation" of $Li_3Ti_2(PO_4)_3$ brings Li_2O_2 passivation to the $LiTi_2(PO_4)_3$, while in "electrochemical oxidation" the Li_2O_2 is deposited on the other side, which hardly affects the self-recovery process.

The XPS spectra of the LOHC (the $LiTi_2(PO_4)_3$ side) obtained before discharging, after discharging in argon and after resting in oxygen are displayed in Fig. 6e and Fig. 6f. As Fig. 6e demonstrates, the Li 1s peak after discharging in argon (~56.1 eV) showed a slight difference comparing to the peak before discharging (~56 eV), which indicates the transformation from $LiTi_2(PO_4)_3$ to $Li_3Ti_2(PO_4)_3$. The Li 1s peak before resting in oxygen was also observed in Kazakevičius et al.s' work[35], in which they noticed the Li 1s peak of ~56 eV from La-doped $LiTi_2(PO_4)_3$, and their result is identical to our observation of the Li 1s peak. The obvious shift of the peak after resting in oxygen (~55 eV) from the peaks in the other two curves suggested the considerable production of Li_2O_2 after the self-recovery. This Li 1s peak of Li_2O_2 was also recognized in many researchers' work about the Li 1s peak in Li_2O_2 XPS spectra[36,37], and they all clearly noted the Li 1s binding energy of around 54.5

eV in Li_2O_2, which is in agreement with our observation of the peak's lower shift. The product Li_2O_2 covered the $LiTi_2(PO_4)_3$ surface, which was in agreement with the SEM images above. In Fig. 6f, the distinct shift of Ti $2p_{3/2}$ peak after discharging in argon (~459.5 eV) comparing to the peak before discharging (~460.3 eV) further reveals the transformation from $LiTi_2(PO_4)_3$ (Ti^{4+}) to $Li_3Ti_2(PO_4)_3$ (Ti^{3+}). These two lithiated/delithiated Ti $2p_{3/2}$ peaks of Ti^{3+} and Ti^{4+} were also noticed in other researcher's XPS spectra[38]. In their work, the lithiated Ti $2p_{3/2}$ peak (Ti^{3+}) was 459.1 eV and the delithiated Ti $2p_{3/2}$ peak (Ti^{4+}) was 459.8 eV, which are quite identical to our results. Therefore the peak after resting in oxygen (~460 eV) between the other two peaks implies the recovery of $LiTi_2(PO_4)_3$ from the $Li_3Ti_2(PO_4)_3$, which is also in agreement with the SEM results.

4. CONCLUSIONS

In summary, a $LiTi_2(PO_4)_3/O_2$ hybrid cathode was designed and established to improve the power performance of LOBs by introducing the carbon-coated NASICON-type $LiTi_2(PO_4)_3$ prepared by a simple sol-gel method. Comparing to common O_2 cathode, the hybrid cathode exhibited considerable power as high as 5.5 $mW \cdot cm^{-2}$ (more than 4 times of LOB cathode power density) at high currents up to 4 $mA \cdot cm^{-2}$ and retained high-energy delivery at low currents as 0.01 $mA \cdot cm^{-2}$. Besides, the discharged hybrid cathode presented the capability of self-recovery to charged-state while resting in oxygen (the capacity recovery percentage kept around 80% in each resting process), and the durability of high-power output was enhanced by this behavior. This work may provide a new approach to promote the development of lithium-oxygen batteries.

ACKNOWLEDGEMENT
This research was supported by the National Natural Science Foundation for Young Scholars of China (No. 21603154).

References

1. F. Wu and G Yushin, *Energ. Environ. Sci.,* 10 (2017) 435.
2. W. Li, B. Song and A. Manthiram, *Chem. Soc. Rev.*, 46 (2017) 3006.
3. G. E. Blomgren, *J. Electrochem. Soc.*, 164 (2017) A5019.
4. J. Lu, T. Wu and K. Amine, *Nat. Energy*, 2 (2017) 17011.
5. S. A. Freunberger, *Nat. Energy*, 2 (2017) 17091.
6. P. G. Bruce, S. A. Freunberger, L. J. Hardwick and J. M. Tarascon, *Nat. Mater.*, 11 (2012) 19.
7. A. C. Luntz and B. D. McCloskey, *Chem. Rev.*, (2014) 11721.
8. X. B. Cheng, R. Zhang, C. Z. Zhao and Q. Zhang, *Chem. Rev.*, 117 (2017) 10403.
9. R. Zhang, N. W. Li, X. B. Cheng, Y. X. Yin, Q. Zhang and Y. G. Guo, *Adv. Sci.*, 4 (2017) 1600445.
10. D. Aurbach, B. D. McCloskey, L. F. Nazar and P. G. Bruce, *Nat. Energy*, 1 (2016) 16128.
11. F. Li and J. Chen, *Adv. Energy Mater.*, 7 (2017) 1602934.
12. M. M. Ottakam Thotiyl, S. A. Freunberger, Z. Peng and P. G. Bruce, *J. Am. Chem. Soc.*, 135 (2012) 494.
13. S. A. Freunberger, Y. Chen, N. E. Drewett, L. Hardwick, F. Barde and P. G. Bruce, *Angew. Chem. Int. Ed.*, 50 (2011) 8609.

14. A. Dunst, V. Epp, I. Hanzu, S. A. Freunberger and M. Wilkening, *Energ. Environ. Sci.*, 7(2014) 2739.
15. H. D. Lim, K. Y. Park, H. Song, E. Y. Jang, H. Gwon, J. Kim, Y. H. Kim, M. D. Lima, R. O. Robles, X. Lepro, R. H. Baughman and K. Kang, *Adv. Mater.*, 25 (2013) 1348.
16. J. J. Xu, Z. L. Wang, D. Xu, L. L. Zhang and X. B. Zhang, *Nat. Commun.*, 4 (2013) 2438.
17. Z. Peng, S. A. Freunberger, Y. Chen and P. G. Bruce, *Science*, (2012) 1223985.
18. F. Tian, M. D. Radin and D. J. Siegel. *Chem. Mater.*, 26 (2014) 2952.
19. A. C. Luntz, V. Viswanathan, J. Voss, J. B. Varley, J. K. Norskov, R. Scheffler and A. Speidel, *J. Phys. Chem. Lett.*, 4 (2013) 3494.
20. Y. Cui, Z. Wen, X. Liang, Y. Lu, J. Jin, M. Wu and X. Wu, *Energ. Environ. Sci.*, 5 (2012) 7893.
21. S. Monaco, F. Soavi and M. Mastragostino, *J. Phys. Chem. Lett.*, 4 (2013) 1379.
22. T. Zhang and H. Zhou, *Angew. Chem. Int. Ed.*, 51 (2012) 11062.
23. Y. C. Lu, H. A. Gasteiger and Y. J. Shao-Horn, *Am. Chem. Soc.*, 133 (2011) 19048.
24. J. Zhang, L. Wang, L. Xu, X. Ge, X. Zhao, M. Lai, Z. Liu and W. Chen, *Nanoscale*, 7 (2015) 720.
25. Y. C. Lu, D. G. Kwabi and K. P. C. Yao, *Energy Environ. Sci.*, 4 (2011) 2999.
26. C. Masquelier and L. Croguennec, *Chem. Rev.*, 113 (2013) 6552.
27. C. Delmas and A. Nadiri, *Mater. Res. Bull.*, 23 (1988) 65.
28. D. Wu, Z. Guo, X. Yin, Q. Pang, B. Tu, L. Zhang, Y. Wang and Q. Li, *Adv. Mater.*, 26 (2014) 3258.
29. X. Chen, P. Kuang, C. Chen, X. Zhang, T. Huang, L. Zhang and A. Yu, *Int. J. Electrochem. Sci.*, 13 (2018) 3309.
30. C. Zhao, C. Yu, S. Liu, J. Yang, X. Fan, H. Huang and J. Qiu, *Adv. Funct. Mater.*, 25 (2015) 6913.
31. K. M. Abraham and Z. Jiang, *J. Electrochem. Soc.*, 143 (1996) 1.
32. D. Xiao, S. Dong, J. Guan, L. Gu, S. Li, N. Zhao, C. Shang, Z. Yang, H. Zheng, C. Chen, R. Xiao, Y. Hu, H. Li, G. Cui and L. Chen, *Adv. Energy Mater.*, 5 (2015) 1400664.
33. J. Luo and Y. Xia, *Adv. Funct. Mater.*, 17 (2007) 3877.
34. J. Read, *J. Electrochem. Soc.*, 149 (2002) A1190.
35. E. Kazakevičius, T. Šalkus, A. Dindune, Z. Kanepe, J. Ronis, A. Kežionis, V. Kazlauskienė, J. Miškinis, A. Selskienė and A. Selskis, *Solid State Ionics*, 179 (2008) 51.
36. S. Zhang, G. Wang, J. Jin, L. Zhang, Z. Wen and J. Yang, *Nano Energy*, 36 (2017) 186.
37. K. P. C. Yao, D. G. Kwabi, R. A. Quinlan, A. N. Mansour, A. Grimaud, Y. L. Lee, Y. C. Lu and Y. Shao-Horn, *J. Electrochem. Soc.*, 160 (2013) A824.
38. S. Wang, Y. Ding, G. Zhou, G. Yu and A. Manthiram, *ACS Energy Lett.*, 1 (2016) 1080.